Accurate bulk properties of nuclei from A=2 to infinity from potentials with Delta isobars

Accurate bulk properties of nuclei from $A = 2$ to ∞ from potentials with Δ isobars

W. G. Jiang,[1,2,3] A. Ekström,[3] C. Forssén,[3] G. Hagen,[2,1] G. R. Jansen,[4,2] and T. Papenbrock[1,2]

[1]*Department of Physics and Astronomy, University of Tennessee, Knoxville, Tennessee 37996, USA*

[2]*Physics Division, Oak Ridge National Laboratory, Oak Ridge, Tennessee 37831, USA*

[3]*Department of Physics, Chalmers University of Technology, SE-412 96 Göteborg, Sweden*

[4]*National Center for Computational Sciences, Oak Ridge National Laboratory, Oak Ridge, Tennessee 37831, USA*

(Received 2 July 2020; revised 26 August 2020; accepted 16 October 2020; published 2 November 2020)

We optimize Δ-full nuclear interactions from chiral effective field theory. The low-energy constants of the contact potentials are constrained by two-body scattering phase shifts, and by properties of bound state of $A = 2$ to 4 nucleon systems and nuclear matter. The pion-nucleon couplings are taken from a Roy-Steiner analysis. The resulting interactions yield accurate binding energies and radii for a range of nuclei from $A = 16$ to $A = 132$, and provide accurate equations of state for nuclear matter and realistic symmetry energies. Selected excited states are also in agreement with data.

DOI: 10.1103/PhysRevC.102.054301

I. INTRODUCTION

Ideas from chiral effective field theory (EFT) and the renormalization group [1–5], advances in computing power, and developments of many-body methods that scale polynomially with mass number, have propelled *ab initio* calculations of atomic nuclei from light [6,7] to medium-mass isotopes [8–16]. Such approaches are now starting to explore ever-increasing fractions of the nuclear chart [17]—a task once thought to be reserved for computationally less expensive mean-field methods [18–20]. *Ab initio* computations make controlled approximations that give a quantifiable precision in the solution of the quantum many-body problem. All these calculations are only as accurate as the employed nuclear Hamiltonians.

In the past two decades, our understanding of the nuclear interactions has evolved from phenomenological models [21,22] to potentials whose improvement is guided by ideas from EFT [3,5,23]. The quest to link such potentials to quantum chromodynamics, the microscopic theory of the strong nuclear interaction, is ongoing [24–27]. Recent developments in nuclear potentials from chiral EFT include (i) the identification [28,29] of a redundant term at next-to-next-to-next-to leading order, (ii) the systematic and simultaneous optimization of nucleon-nucleon and three-nucleon potentials [30,31], (iii) the construction of local potentials for use with quantum Monte Carlo methods [32,33], and (iv) the development of high-order interactions [34–37].

In spite of these advances, nuclear potentials from chiral EFT have long struggled to accurately reproduce bulk nuclear properties such as charge radii and binding energies of finite nuclei, and the saturation point and the symmetry energy of infinite nuclear matter. Notable exceptions are the 1.8/2.0(EM) [38] and the $NN + 3N$(lnl) interactions [39] (which accurately reproduce binding energies and spectra of selected nuclei up to tin isotopes [15] but yield too small radii), and the $\mathrm{NNLO_{sat}}$ potential [30] (which accurately describes binding energies and radii up to calcium isotopes [40] but is less accurate for spectra). The novel family of interactions [41] also seems promising but is not much explored yet. While it is not clear what distinguishes these particular interactions from their many peers that become inaccurate beyond oxygen isotopes [42], some key ingredients to nuclear binding have been uncovered: Nuclear lattice EFT computations revealed that nonlocality is essential for low-momentum interactions (with momentum cutoffs below about 600 MeV) [43], and that elastic α-α scattering, for example, is very sensitive to the degree of nonlocality [44]. This casts some doubts on the viability of soft local interactions. In our interpretation, these results indicate that the finite size of nucleons plays an important role in nuclear binding.[1] The importance of this length scale has been highlighted very recently by Miller [45]. Consistent with this view is the finding that the inclusion of Δ isobar degrees of freedom, i.e., excited states of the nucleon that reflect its finite size, considerably improve the saturation properties of chiral potentials [46]. In addition, a recent statistical analysis [47] reveals that the nuclear radius, i.e., implicitly the nuclear saturation density, depends very sensitively on the details of the chiral interaction. This suggests that it might be profitable to include Δ-isobar degrees of freedom and nuclear matter

[1]The hard core in local interactions also accounts for the finite nucleon size when large momentum cutoffs can be tolerated [21].

TABLE I. Parameters for the new Δ-full potentials with momentum cutoffs $\Lambda = 450$ and 394 MeV. The constants c_i, $\tilde{C}_i$, and C_i are in units of GeV^{-1}, $10^4\,\mathrm{GeV}^{-2}$, and $10^4\,\mathrm{GeV}^{-4}$, respectively.

LEC	$\Delta\mathrm{NLO}_{\mathrm{GO}}(450)$	$\Delta\mathrm{NNLO}_{\mathrm{GO}}(450)$	$\Delta\mathrm{NNLO}_{\mathrm{GO}}(394)$
c_1	–	−0.74	−0.74
c_2	–	−0.49	−0.49
c_3	–	−0.65	−0.65
c_4	–	+0.96	+0.96
$\tilde{C}_{^1S_0}^{(nn)}$	−0.314882	−0.339887	−0.338746
$\tilde{C}_{^1S_0}^{(np)}$	−0.315639	−0.340114	−0.339250
$\tilde{C}_{^1S_0}^{(pp)}$	−0.314300	−0.339111	−0.338142
$\tilde{C}_{^3S_1}$	−0.234132	−0.253950	−0.259839
$C_{^1S_0}$	+2.521650	+2.526636	+2.505389
$C_{^3S_1}$	+1.025459	+0.964990	+1.002189
$C_{^1P_1}$	+0.152206	−0.219498	−0.387960
$C_{^3P_0}$	+0.671880	+0.671908	+0.700499
$C_{^3P_1}$	−0.955644	−0.915398	−0.964856
$C_{^3P_2}$	−0.824639	−0.895405	−0.883122
$C_{^3S_1-{}^3D_1}$	+0.451306	+0.445743	+0.452523
c_D	–	−0.454	+0.081
c_E	–	−0.186	−0.002

properties into the construction and optimization, respectively, of nuclear potentials [48,49].

In this paper we report on chiral potentials that accurately describe bulk properties of finite nuclei and nuclear matter. We optimized Δ-full interactions and included nuclear matter properties as calibration data. We used the coupled-cluster (CC) method to compute ground-state energies, charge radii, and spectra of nuclei up to tin, plus the equation of state for nuclear matter.

II. OPTIMIZATION

The Δ-full interactions are based on Refs. [23,50–53], and its specific form was used in Ref. [46]. We employed standard nonlocal regulator functions $f(p) = \exp\left(p/\Lambda\right)^{2n}$ that act on relative momenta p, see, e.g., Refs. [54,55]. We constructed three potentials: two of them with $\Lambda = 450$ MeV (and power $n = 3$ in the regulator) at next-to-leading order (NLO) and next-to-next-to-leading (NNLO), the other one at NNLO with a cutoff $\Lambda = 394$ MeV (and power $n = 4$). The softer interaction has a momentum cutoff and regulator power exactly as the 1.8/2.0(EM) potential. At NNLO there are 17 low-energy coefficients (LECs) that parametrize the interaction. The pion-nucleon LECs $c_{1,2,3,4}$ were held fixed during the optimization and taken as the central values from the recent Roy-Steiner analysis [56]—see Table I. The LECs of the nucleon-nucleon and three-nucleon potentials were simultaneously constrained by the following data: low-energy nucleon-nucleon scattering data from the Granada phase shift analysis [57] up to 200 MeV scattering energy in the laboratory system; observables of few-nucleon systems (with mass numbers $A \leqslant 4$) as listed in Table II; the saturation energy and density, and constraints

TABLE II. Binding energies (E) in MeV, charge radii (R_{ch}) in fm, for ^{2,3}H and ^{3,4}He computed with the interactions developed in this work and compared to data [64,65]. The quadrupole moment (Q) in $e\mathrm{fm}^2$ for the ground state of ^{2}H is also shown. The D-state probability is 3.06%, 3.12%, and 2.97% for the three interactions in column order.

	$\Delta\mathrm{NLO}_{\mathrm{GO}}$ (450)	$\Delta\mathrm{NNLO}_{\mathrm{GO}}$ (450)	$\Delta\mathrm{NNLO}_{\mathrm{GO}}$ (394)	Exp.
$E(^2\mathrm{H})$	2.2586	2.2358	2.2298	2.2245
$R_{\mathrm{ch}}(^2\mathrm{H})$	2.1511	2.1509	2.1531	2.1421
$Q(^2\mathrm{H})$	0.2680	0.2675	0.2674	0.27[a]
$E(^3\mathrm{H})$	8.4803	8.4809	8.4812	8.4818
$R_{\mathrm{ch}}(^3\mathrm{H})$	1.7928	1.7801	1.7833	1.7591
$E(^3\mathrm{He})$	7.7495	7.7162	7.7245	7.7180
$R_{\mathrm{ch}}(^3\mathrm{He})$	1.9954	2.0036	1.9946	1.9661
$E(^4\mathrm{He})$	28.3945	28.2975	28.3028	28.2957
$R_{\mathrm{ch}}(^4\mathrm{He})$	1.7099	1.6960	1.6919	1.6775

[a]CD-Bonn value according to Ref. [5]. See the text for details.

on the symmetry energy and its slope of nuclear matter from a lower bound on the neutron-matter energy [58]. The inclusion of the latter is in contrast to the construction of the potential $\mathrm{NNLO}_{\mathrm{sat}}$ [30] which exhibits deficiencies for neutron-rich nuclei and neutron matter. The minimization of the objective function was performed with the algorithm POUNDerS [59]. During this process we periodically calculated selected medium-mass nuclei to further guide the optimization. This allowed us to properly adjust the weights of the nuclear matter properties in the objective function

$$f(\vec{x}) = w_1 \sum_{p=1}^{N_p} r_p^2(\vec{x}) + w_2 \sum_{q=1}^{N_q} r_q^2(\vec{x}) + w_3 \sum_{s=1}^{N_s} r_s^2(\vec{x}), \quad (1)$$

where $\vec{x}$ denotes the parameters of the interaction, $r_i(\vec{x}) = (\mathcal{O}_i^{\mathrm{theo}}(\vec{x}) - \mathcal{O}_i^{\mathrm{exp}})/\delta_i$ is the residual of observable $\mathcal{O}_i$ with uncertainty δ_i determining its weight, r_p, r_q, and r_s are the residuals for phase shifts, few-nucleon systems and nuclear matter, respectively, and w_i are their corresponding weights. Note that the weight of the ^{2}H quadrupole moment is increased to improve its description.

The inclusion of nuclear matter properties into the optimization procedure is not without challenges. Here, we used coupled-cluster calculations [60], which are based on a discrete lattice in momentum space. Nondegenerate reference states are "closed shell" configurations, and we used periodic boundary conditions in position space. Systems of 132 nucleons and 66 neutrons exhibit one of the smallest finite-size corrections for symmetric nuclear matter and neutron matter, respectively [60,61]. Unfortunately, such large particle numbers are numerically too expensive to be used in the optimization. However, systems of 28 nucleons and 14 neutrons exhibit predictable differences (about 10%) from systems consisting of 132 and 66 particles, respectively [60]. This allowed us to use the lower-precision computations with smaller system sizes in the optimization. We checked periodically that our estimates for the finite-size corrections were accurate.

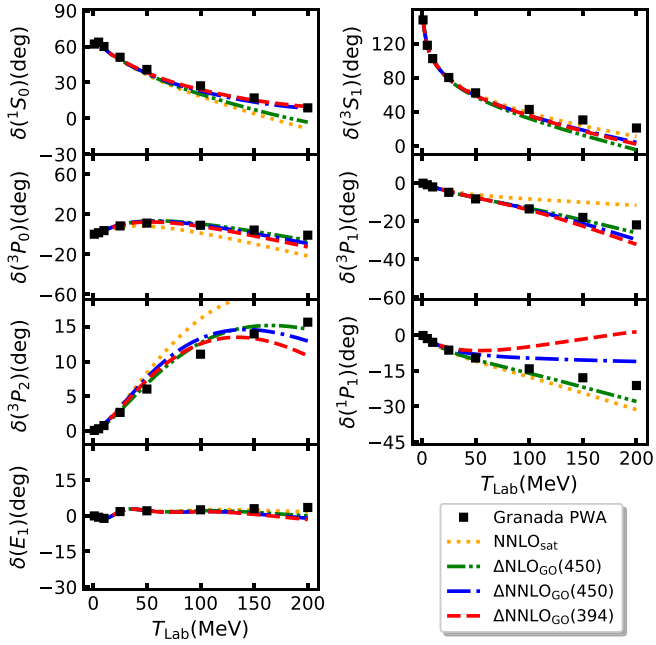

FIG. 1. Computed neutron-proton phase shifts for the contact partial waves with the ΔNLO$_{\rm GO}$ and ΔNNLO$_{\rm GO}$ potentials (dashed), NNLO$_{\rm sat}$ [30] (red, dotted), and compared with the Granada phase shift analysis [57] (black squares).

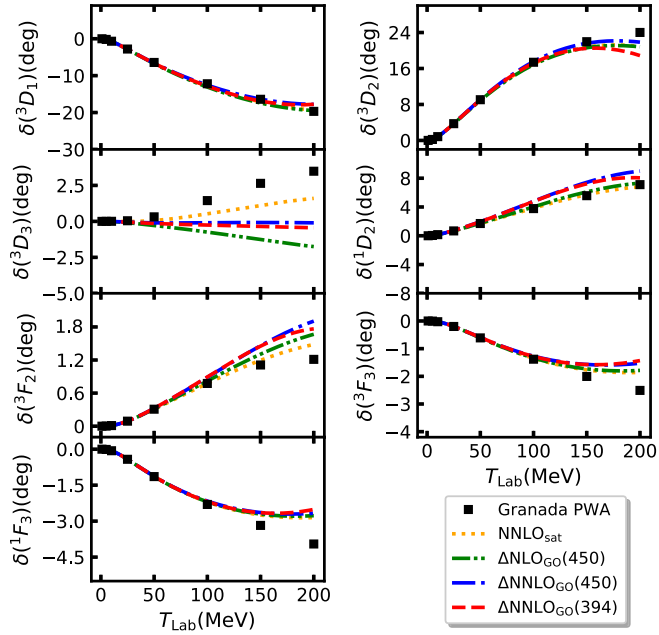

FIG. 2. Computed neutron-proton phase shifts for the selected peripheral partial waves with the ΔNLO$_{\rm GO}$ and ΔNNLO$_{\rm GO}$ potentials (dashed), NNLO$_{\rm sat}$ [30] (red, dotted), and compared with the Granada phase shift analysis [57] (black squares).

To explore the resolution-scale dependence, we optimized the interaction using two cutoffs, namely $\Lambda = 450$ and $\Lambda = 394$ MeV at the NNLO level. For $\Lambda = 450$ MeV we also optimized an NLO interaction. Table I shows the optimized LECs values for the three interactions of this work. In what follows, we label these "Gothenburg–Oak Ridge" potentials as ΔNLO$_{\rm GO}$(450), ΔNNLO$_{\rm GO}$(450), and ΔNNLO$_{\rm GO}$(394). Most of the LECs of the newly constructed potentials are close to the starting point of Ref. [46], with a few exceptions. In particular, the c_D and c_E for the short-ranged three-nucleon forces have different signs for ΔNNLO$_{\rm GO}$(450).

Figures 1, 2, and 3 show the phase shifts of the new potentials for a few representative neutron-proton channels and compares them to the Granada partial wave analysis [57]. Overall, the phase shifts of ΔNNLO$_{\rm GO}$ are improved compared to NNLO$_{\rm sat}$, and they are close to the data for laboratory energies below about 125 MeV. We note that the phase shifts of ΔNLO$_{\rm GO}$(450) are within the uncertainty estimates expected at this order [35,46,62]. One should see that some partial waves such as ^{1}P$_1$ and ^{3}D$_3$ are less accurate than others and might need higher orders of the potentials to give a better description.

Table II summarizes the results of bound-state observables for light nuclei with $A \leqslant 4$. The theoretical results were obtained with the no-core shell model (NCSM) [6] in translationally invariant Jacobi coordinates [63]. These calculations used an oscillator frequency of $\hbar\omega = 36(28)$ MeV for $\Lambda = 450(394)$ MeV in model spaces consisting of $N_{\rm max} = 40$ and $N_{\rm max} = 20$ oscillator shells for $A = 3$ and $A = 4$ nuclei, respectively. They are converged within these model spaces. The charge radii shown in Table II are obtained from the computed point-proton radii with standard nucleon-size and relativistic corrections, see, e.g., Ref. [30]. The two ΔNNLO$_{\rm GO}$ potentials reproduce the experimental energies within less than 0.5% and other observables within 2%. We note that it was important to include the deuteron quadrupole moment as

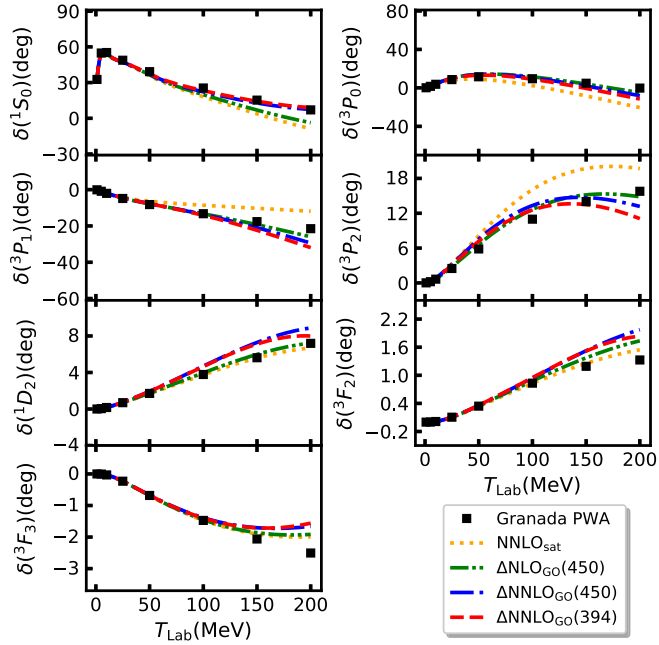

FIG. 3. Computed proton-proton phase shifts for the contact and selected peripheral partial waves with new ΔNLO$_{\rm GO}$ and ΔNNLO$_{\rm GO}$ potentials (dashed), NNLO$_{\rm sat}$ [30] (red, dotted), and compared with the Granada phase shift analysis [57] (black squares).

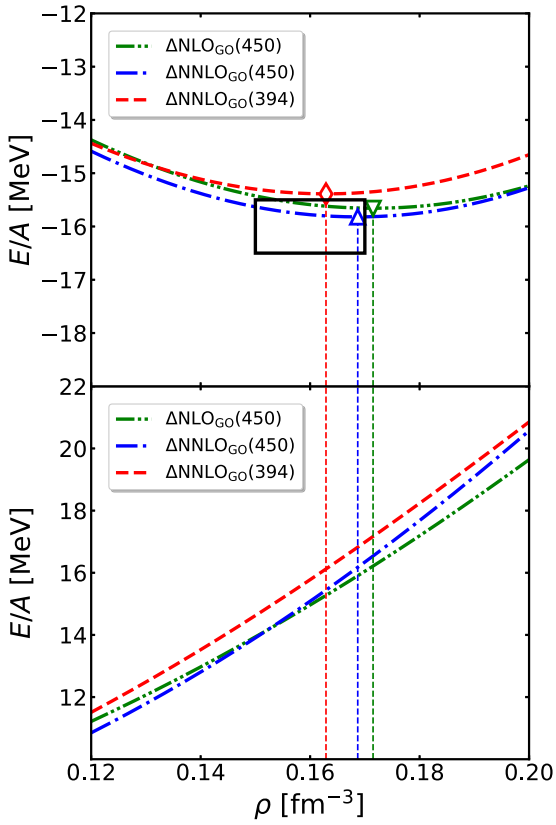

FIG. 4. Energy per nucleon (in MeV) for symmetric nuclear matter (top) and pure neutron matter (bottom) with $\Delta\text{NLO}_{\text{GO}}(450)$, $\Delta\text{NNLO}_{\text{GO}}(450)$, and $\Delta\text{NNLO}_{\text{GO}}(394)$. The black rectangle indicates the empirical saturation point.

a calibration datum in the optimization. The value for the quadrupole moment that we targeted, i.e., $Q = 0.27\,e\text{fm}^2$, was obtained from a theoretical calculation based on the high-precision meson-exchange NN model CD-Bonn.

Figure 4 shows the energy per nucleon in symmetric nuclear matter (top) and pure neutron matter (bottom) as a function of density, using 132 nucleons and 66 neutrons, respectively. The black rectangle indicates the empirical saturation region with $E/A = -16 \pm 0.5$ MeV and $\rho = 0.16 \pm 0.01$ fm^{-3} [38,66]. The CC calculations were performed in the CCD(T) approximation, i.e., with $2p$-$2h$ excitations and perturbative $3p$-$3h$ corrections as done in Refs. [46,60]. We find the saturation density $\rho_0 = 0.169$ fm^{-3}, the symmetry energy $S_0 = 32.0$ MeV and its slope $L = 65.2$ for the $\Delta\text{NNLO}_{\text{GO}}(450)$ potential, and $\rho_0 = 0.163$ fm^{-3}, $S_0 = 31.5$ MeV, and $L = 58.4$ for $\Delta\text{NNLO}_{\text{GO}}(394)$. These nuclear-matter properties are more accurate than those reported in Ref. [46], and in good agreement with the recent predictions of the symmetry energy and its slope obtained using Bayesian machine learning techniques to quantify EFT uncertainties of the nuclear matter equation of state [67].

III. RESULTS

Our CC computations of heavier nuclei started from a spherical Hartree-Fock state built from a model-space consisting of 15 major oscillator shells with frequency $\hbar\omega = 16$ MeV. The three-nucleon force had the additional energy cut of $E_{3\text{max}} = 16\hbar\omega$. Our calculations employed the coupled-cluster singles, doubles, and leading triples approximation CCSDT-1 [68]. No further truncations were imposed on the three-particle–three-hole amplitudes. This computational achievement was enabled by the Nuclear Tensor Contraction Library [69]—a domain-specific library, dedicated to the sparse tensor contractions that dominate in coupled-cluster method—that is developed to run at scale on Summit, the U.S. Department of Energy's 200 petaflop supercomputer operated by the Oak Ridge Leadership Computing Facility (OLCF) at Oak Ridge National Laboratory.

TABLE III. Binding energies (in MeV) for selected nuclei with the new interaction using CCSDT-1 and compared to data.

	$\Delta\text{NLO}_{\text{GO}}$ (450)	$\Delta\text{NNLO}_{\text{GO}}$ (450)	$\Delta\text{NNLO}_{\text{GO}}$ (394)	Exp.
^{16}O	128.2	128.1(23)	127.5(19)	127.62
^{24}O	165	170 (3)	169 (3)	168.96
^{40}Ca	341	348 (7)(1)	346 (6)	342.05
^{48}Ca	410	422 (9)(4)	420 (7)	416.00
^{78}Ni	–	631 (14)(20)	639 (11)(4)	641.55
^{90}Zr	–	–	782 (14)(6)	783.90
^{100}Sn	–	–	818 (16)(7)	825.30
^{132}Sn	–	–	1043 (20)(30)	1102.84

Table III shows the binding energies of selected closed-shell nuclei up to ^{132}Sn. We found that $\Delta\text{NNLO}_{\text{GO}}(394)$ converges faster, especially for heavier nuclei, than $\Delta\text{NNLO}_{\text{GO}}(450)$. This is expected due to its lower momentum cutoff. A dash indicates that the employed model space was too small to achieve reasonably converged energies. Uncertainties from the coupled-cluster method (about 30% of the difference between doubles and triples energies) and from the model space are given in subsequent parenthesis, respectively. For lighter nuclei, the uncertainties from the model-space are omitted because they are much smaller than those of the method. The model-space uncertainties combine the truncation of single-particle model space and the employed $E_{3\text{max}} = 16$ cut of the three-nucleon interaction. Reference [15] found that for the 1.8/2.0(EM) interaction the binding energy of ^{100}Sn changes by less than 1% by increasing $E_{3\text{max}}$ from $E_{3\text{max}} = 16$ to $E_{3\text{max}} = 18$. This finding guided our estimated model-space uncertainty as the 1.8/2.0(EM) has identical three-nucleon regulator and momentum cutoff as the $\Delta\text{NNLO}_{\text{GO}}(394)$ potential. It is nontrivial to estimate the EFT truncation errors for bound nuclear states since the relevant momentum scale is unknown and the lack of a spin-orbit (LS) force at leading order (LO) give energy degeneracies that hamper CC calculations of non-LS-closed nuclei. Nevertheless, based on the observed order-by-order convergence in Ref. [46], we estimate the EFT truncation errors for the $\Delta\text{NNLO}_{\text{GO}}$ interactions to 1 MeV and 7 MeV in the ground state energies of oxygen and calcium isotopes, respectively. We also expect the truncation error to be the dominating source of uncertainty in heavier

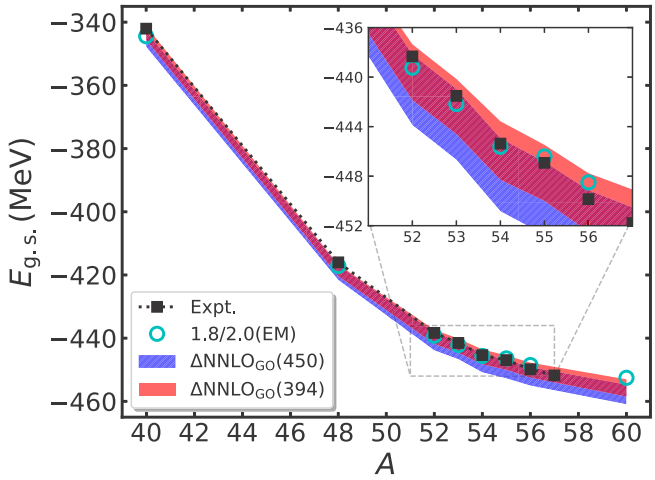

FIG. 5. The ground-state energies of calcium isotopes obtained with ΔNNLO$_{GO}$ and 1.8/2.0(EM) interaction compared with experiment (data of $^{55-57}$Ca are taken from Ref. [74]).

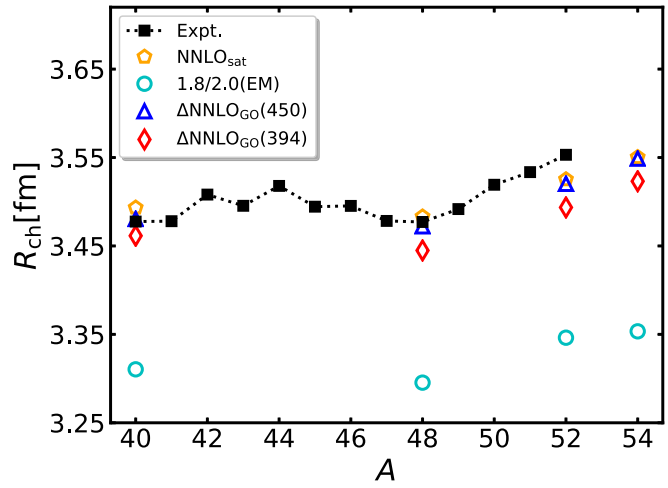

FIG. 6. Charge radii of calcium isotopes obtained with with ΔNNLO$_{GO}$ and 1.8/2.0(EM) interaction compared with experiment.

nuclei. For symmetric nuclear matter and pure neutron matter we expect a truncation error of ±1 MeV and ±2 MeV per nucleon, respectively, with ΔNNLO$_{GO}$, see Ref. [46] for details.

Figure 5 shows the ground-state energies of selected calcium isotopes and compares them to the 1.8/2.0(EM) interaction [70] and to data. The lower borders of the bands are results from CCSDT-1 while the upper borders are from Λ-CCSD(T) [71] which treats triples excitations perturbatively. For ^{53,55}Ca we employed the particle-attached equation-of-motion coupled-cluster (EOM-CC) method with perturbative three-particle–two-hole excitations from Ref. [15], while for ^{56}Ca we employed the two-particle attached EOM-CC method from Refs. [72,73]. All interactions accurately describe isotopes from ^{40}Ca to ^{56}Ca. We note that the ground state of ^{60}Ca is bound by about 10 MeV with respect to ^{54}Ca, consistent with recent data [74–76].

Figure 6 shows that the interactions of this work yield significantly larger charge radii than the 1.8/2.0(EM) potential. Nevertheless, the ΔNNLO$_{GO}$ potentials still fail to explain the unusually large charge radii of neutron-rich calcium isotopes. For speculations about the origin of these large charge radii in calcium isotopes we refer the reader to Ref. [77].

We employed EOM-CC methods with singles, doubles, and leading-order triples excitations, EOM-CCSDT-1 [78], to compute excited states of ^{16,22,24}O and ^{48}Ca. The EOM-CCSDT-1 method is computationally demanding, and we therefore limited the number of three-particle–three-hole excitations by employing the energy cut $\tilde{E}_{pqr} = \tilde{e}_p + \tilde{e}_q + \tilde{e}_r < \tilde{E}_{3\max}$, where $\tilde{e}_p = |N_p - N_F|$ is the energy difference of the single-particle energies with respect to the Fermi surface N_F. This energy cut improved the convergence of the EOM-CCSDT-1 method with respect to the number of three-particle–three-hole excitations [79,80]. In this work we also employed the method developed in Ref. [80] to correct perturbatively for three-particle–three-hole excitations above $\tilde{E}_{3\max}$. Here, we employed the energy cut $\tilde{E}_{3\max} = 6$ which was sufficient to converge all excited states to within approximately 100 keV. The results are summarized in Table IV with estimated error bars. The ΔNNLO$_{GO}$(450) potential only exhibits marginal agreement with the data for ^{22}O. In contrast, all potentials accurately reproduce the first 3^- state of ^{16}O which reflects that the charge radius is well reproduced in this nucleus (see Ref. [30] for a more detailed discussion on this point). The uncertainties are estimated based on Refs. [80,81]. Here, excited states were computed in different truncations within the EOM-CC approach, and it was found that the triples correction to the excited states were about 20% of the EOM-CCSD correlation energy. Using this, we give a conservative error estimate in the first parenthesis which amounts to 6% and 15% of the total excitation energies for the interactions with cutoffs 394 MeV and 450 MeV, respectively. The uncertainties from the truncated model space are given in the second parenthesis.

Finally we note that the potentials developed in this work have recently been applied to several other open-shell and deformed nuclei such as ^{29}F [82], ^{40}Ar [83], and neon and magnesium isotopes [84].

TABLE IV. Energies (in MeV) of selected excited states for different nuclei using ΔNNLO$_{GO}$(450) and ΔNNLO$_{GO}$(394) with EOM-CCSDT-1 and compared to experiment. The uncertainties reflect estimated equation-of-motion coupled-cluster and model-space truncation errors, respectively.

	ΔNNLO$_{GO}$(450)	ΔNNLO$_{GO}$(394)	Exp.
^{16}O 3^-_1	6(1)	5.6(3)(1)	6.13
^{22}O 2^+_1	2.2(3)(1)	3.0(2)(1)	3.20
^{24}O 2^+_1	3.4(5)(2)	3.9(2)(1)	4.79
^{48}Ca 2^+_1	3.5(5)(2)	4.1(2)(1)	3.83

IV. SUMMARY

We developed chiral interactions with Δ degrees of freedom by calibrating LECs to reproduce nucleon-nucleon scattering phase shifts, bound-state observables of few-nucleon systems, and properties of infinite nuclear matter. The resulting $\Delta\text{NNLO}_{\text{GO}}$ potentials yield accurate (within about 2%) binding energies of nuclei up to mass numbers $A = 132$, and improved radii for medium-mass nuclei. The description of neutron-rich calcium isotopes is improved by including the symmetry energy in the optimization. Selected excited states are also accurately reproduced. This shows that key nuclear properties can be obtained by chiral interactions at next-to-next-to-leading order.

ACKNOWLEDGMENTS

We thank Titus Morris and Ragnar Stroberg for fruitful discussions, in addition we also thank Ragnar Stroberg for providing us with the 1.8/2.0(EM) results for calcium isotopes. W.J. acknowledges support from FRIB-China Scholarship Council. This work was supported by the Office of Nuclear Physics, U.S. Department of Energy, under Grants No. de-sc0018223 (SciDAC-4 NUCLEI collaboration), No. DE- FG02-96ER40963, and by the Field Work Proposal ERKBP72 at Oak Ridge National Laboratory (ORNL), the European Research Council (ERC) under the European Unions Horizon 2020 research and innovation programme (Grant Agreement No. 758027), the Swedish Research Council (Grant No. 2017-04234), and the Swedish Foundation for International Cooperation in Research and Higher Education (STINT, IG2012-5158). Computer time was provided by the Innovative and Novel Computational Impact on Theory and Experiment (INCITE) program. This research used resources of the Oak Ridge Leadership Computing Facility and of the Compute and Data Environment for Science (CADES) located at ORNL, which is supported by the Office of Science of the Department of Energy under Contract No. DE AC05-00OR22725.

[1] U. Van Kolck, Effective field theory of nuclear forces, Prog. Part. Nucl. Phys. **43**, 337 (1999).
[2] S. K. Bogner, T. T. S. Kuo, and A. Schwenk, Model-independent low momentum nucleon interaction from phase shift equivalence, Phys. Rep. **386**, 1 (2003).
[3] E. Epelbaum, H.-W. Hammer, and Ulf-G. Meißner, Modern theory of nuclear forces, Rev. Mod. Phys. **81**, 1773 (2009).
[4] S. K. Bogner, R. J. Furnstahl, and A. Schwenk, From low-momentum interactions to nuclear structure, Prog. Part. Nucl. Phys. **65**, 94 (2010).
[5] R. Machleidt and D. R. Entem, Chiral effective field theory and nuclear forces, Phys. Rep. **503**, 1 (2011).
[6] B. R. Barrett, P. Navrátil, and J. P. Vary, *Ab initio* no core shell model, Prog. Part. Nucl. Phys. **69**, 131 (2013).
[7] J. Carlson, S. Gandolfi, F. Pederiva, S. C. Pieper, R. Schiavilla, K. E. Schmidt, and R. B. Wiringa, Quantum Monte Carlo methods for nuclear physics, Rev. Mod. Phys. **87**, 1067 (2015).
[8] W. H. Dickhoff and C. Barbieri, Self-consistent Green's function method for nuclei and nuclear matter, Prog. Part. Nucl. Phys. **52**, 377 (2004).
[9] H. Hergert, S. K. Bogner, S. Binder, A. Calci, J. Langhammer, R. Roth, and A. Schwenk, In-medium similarity renormalization group with chiral two- plus three-nucleon interactions, Phys. Rev. C **87**, 034307 (2013).
[10] V. Somà, A. Cipollone, C. Barbieri, P. Navrátil, and T. Duguet, Chiral two- and three-nucleon forces along medium-mass isotope chains, Phys. Rev. C **89**, 061301(R) (2014).
[11] T. A. Lähde, E. Epelbaum, H. Krebs, D. Lee, Ulf-G. Meißner, and G. Rupak, Lattice effective field theory for medium-mass nuclei, Phys. Lett. B **732**, 110 (2014).
[12] G. Hagen, T. Papenbrock, M. Hjorth-Jensen, and D. J. Dean, Coupled-cluster computations of atomic nuclei, Rep. Prog. Phys. **77**, 096302 (2014).
[13] H. Hergert, S. K. Bogner, T. D. Morris, A. Schwenk, and K. Tsukiyama, The in-medium similarity renormalization group: A novel ab initio method for nuclei, Phys. Rep. **621**, 165 (2016).
[14] S. R. Stroberg, A. Calci, H. Hergert, J. D. Holt, S. K. Bogner, R. Roth, and A. Schwenk, Nucleus-Dependent Valence-Space Approach to Nuclear Structure, Phys. Rev. Lett. **118**, 032502 (2017).
[15] T. D. Morris, J. Simonis, S. R. Stroberg, C. Stumpf, G. Hagen, J. D. Holt, G. R. Jansen, T. Papenbrock, R. Roth, and A. Schwenk, Structure of the Lightest Tin Isotopes, Phys. Rev. Lett. **120**, 152503 (2018).
[16] D. Lonardoni, J. Carlson, S. Gandolfi, J. E. Lynn, K. E. Schmidt, A. Schwenk, and X. B. Wang, Properties of Nuclei up to $a = 16$ Using Local Chiral Interactions, Phys. Rev. Lett. **120**, 122502 (2018).
[17] J. D. Holt, S. R. Stroberg, A. Schwenk, and J. Simonis, *Ab initio* limits of atomic nuclei, arXiv:1905.10475 [nucl-th].
[18] J. Erler, N. Birge, M. Kortelainen, W. Nazarewicz, E. Olsen, A. M. Perhac, and M. Stoitsov, The limits of the nuclear landscape, Nature **486**, 509 (2012).
[19] S. E. Agbemava, A. V. Afanasjev, D. Ray, and P. Ring, Global performance of covariant energy density functionals: Ground state observables of even-even nuclei and the estimate of theoretical uncertainties, Phys. Rev. C **89**, 054320 (2014).
[20] S. Shen, H. Liang, W. H. Long, J. Meng, and P. Ring, Towards an *ab initio* covariant density functional theory for nuclear structure, Prog. Part. Nucl. Phys. **109**, 103713 (2019).
[21] R. B. Wiringa, V. G. J. Stoks, and R. Schiavilla, Accurate nucleon-nucleon potential with charge-independence breaking, Phys. Rev. C **51**, 38 (1995).
[22] R. Machleidt, High-precision, charge-dependent Bonn nucleon-nucleon potential, Phys. Rev. C **63**, 024001 (2001).
[23] U. van Kolck, Few-nucleon forces from chiral Lagrangians, Phys. Rev. C **49**, 2932 (1994).
[24] N. Barnea, L. Contessi, D. Gazit, F. Pederiva, and U. van Kolck, Effective Field Theory for Lattice Nuclei, Phys. Rev. Lett. **114**, 052501 (2015).
[25] L. Contessi, A. Lovato, F. Pederiva, A. Roggero, J. Kirscher, and U. van Kolck, Ground-state properties of 4He and 16O extrapolated from lattice QCD with pionless EFT, Phys. Lett. B **772**, 839 (2017).

[26] C. McIlroy, C. Barbieri, T. Inoue, T. Doi, and T. Hatsuda, Doubly magic nuclei from lattice QCD forces at $M_{\rm ps} = 469$ Mev/c^2, Phys. Rev. C **97**, 021303(R) (2018).

[27] A. Bansal, S. Binder, A. Ekström, G. Hagen, G. R. Jansen, and T. Papenbrock, Pion-less effective field theory for atomic nuclei and lattice nuclei, Phys. Rev. C **98**, 054301 (2018).

[28] P. Reinert, H. Krebs, and E. Epelbaum, Semilocal momentum-space regularized chiral two-nucleon potentials up to fifth order, Eur. Phys. J. A **54**, 86 (2018).

[29] S. Wesolowski, R. J. Furnstahl, J. A. Melendez, and D. R. Phillips, Exploring Bayesian parameter estimation for chiral effective field theory using nucleon–nucleon phase shifts, J. Phys. G: Nucl. Part. Phys. **46**, 045102 (2019).

[30] A. Ekström, G. R. Jansen, K. A. Wendt, G. Hagen, T. Papenbrock, B. D. Carlsson, C. Forssén, M. Hjorth-Jensen, P. Navrátil, and W. Nazarewicz, Accurate nuclear radii and binding energies from a chiral interaction, Phys. Rev. C **91**, 051301(R) (2015).

[31] B. D. Carlsson, A. Ekström, C. Forssén, D. F. Strömberg, G. R. Jansen, O. Lilja, M. Lindby, B. A. Mattsson, and K. A. Wendt, Uncertainty Analysis and Order-By-Order Optimization of Chiral Nuclear Interactions, Phys. Rev. X **6**, 011019 (2016).

[32] A. Gezerlis, I. Tews, E. Epelbaum, S. Gandolfi, K. Hebeler, A. Nogga, and A. Schwenk, Quantum Monte Carlo calculations with Chiral Effective Field Theory Interactions, Phys. Rev. Lett. **111**, 032501 (2013).

[33] M. Piarulli, L. Girlanda, R. Schiavilla, R. N. Pérez, J. E. Amaro, and E. R. Arriola, Minimally nonlocal nucleon-nucleon potentials with chiral two-pion exchange including Δ resonances, Phys. Rev. C **91**, 024003 (2015).

[34] D. R. Entem, N. Kaiser, R. Machleidt, and Y. Nosyk, Peripheral nucleon-nucleon scattering at fifth order of chiral perturbation theory, Phys. Rev. C **91**, 014002 (2015).

[35] E. Epelbaum, H. Krebs, and U.-G. Meißner, Precision Nucleon-Nucleon Potential at Fifth Order in the Chiral Expansion, Phys. Rev. Lett. **115**, 122301 (2015).

[36] K. Hebeler, H. Krebs, E. Epelbaum, J. Golak, and R. Skibiński, Efficient calculation of chiral three-nucleon forces up to n^{3}LO for *ab initio* studies, Phys. Rev. C **91**, 044001 (2015).

[37] K. Hebeler, Three-nucleon forces: Implementation and applications to atomic nuclei and dense matter, arXiv:2002.09548 [nucl-th].

[38] K. Hebeler, S. K. Bogner, R. J. Furnstahl, A. Nogga, and A. Schwenk, Improved nuclear matter calculations from chiral low-momentum interactions, Phys. Rev. C **83**, 031301(R) (2011).

[39] V. Somà, P. Navrátil, F. Raimondi, C. Barbieri, and T. Duguet, Novel chiral Hamiltonian and observables in light and medium-mass nuclei, Phys. Rev. C **101**, 014318 (2020).

[40] G. Hagen, A. Ekström, C. Forssén, G. R. Jansen, W. Nazarewicz, T. Papenbrock, K. A. Wendt, S. Bacca, N. Barnea, B. Carlsson, C. Drischler, K. Hebeler, M. Hjorth-Jensen, M. Miorelli, G. Orlandini, A. Schwenk, and J. Simonis, Neutron and weak-charge distributions of the ^{48}Ca nucleus, Nat. Phys. **12**, 186 (2016).

[41] T. Hüther, K. Vobig, K. Hebeler, R. Machleidt, and R. Roth, Family of chiral two- plus three-nucleon interactions for accurate nuclear structure studies, Phys. Lett. B **808**, 135651 (2020).

[42] S. Binder, J. Langhammer, A. Calci, and R. Roth, *Ab initio* path to heavy nuclei, Phys. Lett. B **736**, 119 (2014).

[43] B.-N. Lu, N. Li, S. Elhatisari, D. Lee, E. Epelbaum, and U.-G. Meißner, Essential elements for nuclear binding, Phys. Lett. B **797**, 134863 (2019).

[44] S. Elhatisari, N. Li, A. Rokash, J. M. Alarcón, D. Du, N. Klein, B.-N. Lu, Ulf-G. Meißner, E. Epelbaum, H. Krebs, T. A. Lähde, D. Lee, and G. Rupak, Nuclear Binding Near a Quantum Phase Transition, Phys. Rev. Lett. **117**, 132501 (2016).

[45] G. A. Miller, Discovery vs. precision in nuclear physics- A tale of three scales, arXiv:2008.06524.

[46] A. Ekström, G. Hagen, T. D. Morris, T. Papenbrock, and P. D. Schwartz, Δ isobars and nuclear saturation, Phys. Rev. C **97**, 024332 (2018).

[47] A. Ekström and G. Hagen, Global Sensitivity Analysis of Bulk Properties of an Atomic Nucleus, Phys. Rev. Lett. **123**, 252501 (2019).

[48] J. Simonis, S. R. Stroberg, K. Hebeler, J. D. Holt, and A. Schwenk, Saturation with chiral interactions and consequences for finite nuclei, Phys. Rev. C **96**, 014303 (2017).

[49] C. Drischler, K. Hebeler, and A. Schwenk, Chiral Interactions up to Next-to-Next-to-Next-to-Leading Order and Nuclear Saturation, Phys. Rev. Lett. **122**, 042501 (2019).

[50] T. R. Hemmert, B. R. Holstein, and J. Kambor, Heavy baryon chiral perturbation theory with light deltas, J. Phys. G: Nucl. Part. Phys. **24**, 1831 (1998).

[51] N. Kaiser, S. Gerstendörfer, and W. Weise, Peripheral nn-scattering: Role of delta-excitation, correlated two-pion and vector meson exchange, Nucl. Phys. A **637**, 395 (1998).

[52] H. Krebs, E. Epelbaum, and U. G. Meißner, Nuclear forces with Δ excitations up to next-to-next-to-leading order, Part I: Peripheral nucleon-nucleon waves, Eur. Phys. J. A **32**, 127 (2007).

[53] E. Epelbaum, H. Krebs, and U.-G. Meißner, Δ-excitations and the three-nucleon force, Nucl. Phys. A **806**, 65 (2008).

[54] D. R. Entem and R. Machleidt, Accurate charge-dependent nucleon-nucleon potential at fourth order of chiral perturbation theory, Phys. Rev. C **68**, 041001(R) (2003).

[55] E. Epelbaum, A. Nogga, W. Glöckle, H. Kamada, U.-G. Meißner, and H. Witała, Three-nucleon forces from chiral effective field theory, Phys. Rev. C **66**, 064001 (2002).

[56] D. Siemens, J. R. de Elvira, E. Epelbaum, M. Hoferichter, H. Krebs, B. Kubis, and U.-G. Meißner, Reconciling threshold and subthreshold expansions for pion-nucleon scattering, Phys. Lett. B **770**, 27 (2017).

[57] R. N. Pérez, J. E. Amaro, and E. R. Arriola, Coarse-grained potential analysis of neutron-proton and proton-proton scattering below the pion production threshold, Phys. Rev. C **88**, 064002 (2013).

[58] I. Tews, J. M. Lattimer, A. Ohnishi, and E. E. Kolomeitsev, Symmetry parameter constraints from a lower bound on neutron-matter energy, Astrophys. J. **848**, 105 (2017).

[59] M. Kortelainen, T. Lesinski, J. Moré, W. Nazarewicz, J. Sarich, N. Schunck, M. V. Stoitsov, and S. Wild, Nuclear energy density optimization, Phys. Rev. C **82**, 024313 (2010).

[60] G. Hagen, T. Papenbrock, A. Ekström, K. A. Wendt, G. Baardsen, S. Gandolfi, M. Hjorth-Jensen, and C. J. Horowitz, Coupled-cluster calculations of nucleonic matter, Phys. Rev. C **89**, 014319 (2014).

[61] S. Gandolfi, A. Yu. Illarionov, K. E. Schmidt, F. Pederiva, and S. Fantoni, Quantum Monte Carlo calculation of the equation of state of neutron matter, Phys. Rev. C **79**, 054005 (2009).

[62] R. J. Furnstahl, N. Klco, D. R. Phillips, and S. Wesolowski, Quantifying truncation errors in effective field theory, Phys. Rev. C **92**, 024005 (2015).

[63] P. Navrátil, G. P. Kamuntavičius, and B. R. Barrett, Few-nucleon systems in a translationally invariant harmonic oscillator basis, Phys. Rev. C **61**, 044001 (2000).

[64] I. Angeli and K. P. Marinova, Table of experimental nuclear ground state charge radii: An update, At. Data Nucl. Data Tables **99**, 69 (2013).

[65] M. Wang, G. Audi, F. G. Kondev, W. J. Huang, S. Naimi, and X. Xu, The AME2016 atomic mass evaluation (ii). Tables, graphs and references, Chin. Phys. C **41**, 030003 (2017).

[66] M. Bender, P.-H. Heenen, and P.-G. Reinhard, Self-consistent mean-field models for nuclear structure, Rev. Mod. Phys. **75**, 121 (2003).

[67] C. Drischler, R. J. Furnstahl, J. A. Melendez, and D. R. Phillips, How well do we know the neutron-matter equation of state at the densities inside neutron stars? A Bayesian approach with correlated uncertainties, arXiv:2004.07232 [nucl-th].

[68] Y. S. Lee, S. A. Kucharski, and R. J. Bartlett, A coupled cluster approach with triple excitations, J. Chem. Phys. **81**, 5906 (1984).

[69] NTCL–Nuclear Tensor Contraction Library, https://github.com/gustav-jansen/ntcl.

[70] S. R. Stroberg (private communication) (2020).

[71] A. G. Taube and R. J. Bartlett, Improving upon CCSD(T): Λ-CCSD(T). I. Potential energy surfaces, J. Chem. Phys. **128**, 044110 (2008).

[72] G. R. Jansen, M. Hjorth-Jensen, G. Hagen, and T. Papenbrock, Toward open-shell nuclei with coupled-cluster theory, Phys. Rev. C **83**, 054306 (2011).

[73] G. R. Jansen, Spherical coupled-cluster theory for open-shell nuclei, Phys. Rev. C **88**, 024305 (2013).

[74] S. Michimasa, M. Kobayashi, Y. Kiyokawa, S. Ota, D. S. Ahn, H. Baba, G. P. A. Berg, M. Dozono, N. Fukuda, T. Furuno, E. Ideguchi, N. Inabe, T. Kawabata, S. Kawase, K. Kisamori, K. Kobayashi, T. Kubo, Y. Kubota, C. S. Lee, M. Matsushita, H. Miya, A. Mizukami, H. Nagakura, D. Nishimura, H. Oikawa, H. Sakai, Y. Shimizu, A. Stolz, H. Suzuki, M. Takaki, H. Takeda, S. Takeuchi, H. Tokieda, T. Uesaka, K. Yako, Y. Yamaguchi, Y. Yanagisawa, R. Yokoyama, K. Yoshida, and S. Shimoura, Magic nature of neutrons in ^{54}Ca: First Mass Measurements of $^{55–57}$Ca, Phys. Rev. Lett. **121**, 022506 (2018).

[75] O. B. Tarasov, D. S. Ahn, D. Bazin, N. Fukuda, A. Gade, M. Hausmann, N. Inabe, S. Ishikawa, N. Iwasa, K. Kawata, T. Komatsubara, T. Kubo, K. Kusaka, D. J. Morrissey, M. Ohtake, H. Otsu, M. Portillo, T. Sakakibara, H. Sakurai, H. Sato, B. M. Sherrill, Y. Shimizu, A. Stolz, T. Sumikama, H. Suzuki, H. Takeda, M. Thoennessen, H. Ueno, Y. Yanagisawa, and K. Yoshida, Discovery of ^{60}Ca and Implications for the Stability of ^{70}Ca, Phys. Rev. Lett. **121**, 022501 (2018).

[76] M. L. Cortés, W. Rodriguez, P. Doornenbal, A. Obertelli, J. D. Holt, S. M. Lenzi, J. Menéndez, F. Nowacki, K. Ogata, A. Poves, T. R. Rodríguez, A. Schwenk, J. Simonis, S. R. Stroberg, K. Yoshida, L. Achouri, H. Baba, F. Browne, D. Calvet, F. Château, S. Chen, N. Chiga, A. Corsi, A. Delbart, J.-M. Gheller, A. Giganon, A. Gillibert, C. Hilaire, T. Isobe, T. Kobayashi, Y. Kubota, V. Lapoux, H. N. Liu, T. Motobayashi, I. Murray, H. Otsu, V. Panin, N. Paul, H. Sakurai, M. Sasano, D. Steppenbeck, L. Stuhl, Y. L. Sun, Y. Togano, T. Uesaka, K. Wimmer, K. Yoneda, O. Aktas, T. Aumann, L. X. Chung, F. Flavigny, S. Franchoo, I. Gapari, R.-B. Gerst, J. Gibelin, K. I. Hahn, D. Kim, T. Koiwai, Y. Kondo, P. Koseoglou, J. Lee, C. Lehr, B. D. Linh, T. Lokotko, M. MacCormick, K. Moschner, T. Nakamura, S. Y. Park, D. Rossi, E. Sahin, D. Sohler, P.-A. Söderström, S. Takeuchi, H. Toernqvist, V. Vaquero, V. Wagner, S. Wang, V. Werner, X. Xu, H. Yamada, D. Yan, Z. Yang, M. Yasuda, and L. Zanetti, Shell evolution of $N = 40$ isotones towards ^{60}Ca: First spectroscopy of ^{62}Ti, Phys. Lett. B **800**, 135071 (2020).

[77] R. F. Garcia Ruiz, M. L. Bissell, K. Blaum, A. Ekström, N. Frömmgen, G. Hagen, M. Hammen, K. Hebeler, J. D. Holt, G. R. Jansen, M. Kowalska, K. Kreim, W. Nazarewicz, R. Neugart, G. Neyens, W. Nörtershäuser, T. Papenbrock, J. Papuga, A. Schwenk, J. Simonis, K. A. Wendt, and D. T. Yordanov, Unexpectedly large charge radii of neutron-rich calcium isotopes, Nat. Phys. **12**, 594 (2016).

[78] J. D. Watts and R. J. Bartlett, Economical triple excitation equation-of-motion coupled-cluster methods for excitation energies, Chem. Phys. Lett. **233**, 81 (1995).

[79] M. Miorelli, S. Bacca, G. Hagen, and T. Papenbrock, Computing the dipole polarizability of ^{48}Ca with increased precision, Phys. Rev. C **98**, 014324 (2018).

[80] P. Gysbers, G. Hagen, J. D. Holt, G. R. Jansen, T. D. Morris, P. Navrátil, T. Papenbrock, S. Quaglioni, A. Schwenk, S. R. Stroberg, and K. A. Wendt, Discrepancy between experimental and theoretical b-decay rates resolved from first principles, Nat. Phys. **15**, 428 (2019).

[81] G. Hagen, M. Hjorth-Jensen, G. R. Jansen, and T. Papenbrock, Emergent properties of nuclei from ab initio coupled-cluster calculations, Phys. Scr. **91**, 063006 (2016).

[82] S. Bagchi, R. Kanungo, Y. K. Tanaka, H. Geissel, P. Doornenbal, W. Horiuchi, G. Hagen, T. Suzuki, N. Tsunoda, D. S. Ahn, H. Baba, K. Behr, F. Browne, S. Chen, M. L. Cortés, A. Estradé, N. Fukuda, M. Holl, K. Itahashi, N. Iwasa, G. R. Jansen, W. G. Jiang, S. Kaur, A. O. Macchiavelli, S. Y. Matsumoto, S. Momiyama, I. Murray, T. Nakamura, S. J. Novario, H. J. Ong, T. Otsuka, T. Papenbrock, S. Paschalis, A. Prochazka, C. Scheidenberger, P. Schrock, Y. Shimizu, D. Steppenbeck, H. Sakurai, D. Suzuki, H. Suzuki, M. Takechi, H. Takeda, S. Takeuchi, R. Taniuchi, K. Wimmer, and K. Yoshida, Two-Neutron Halo is Unveiled in ^{29}F, Phys. Rev. Lett. **124**, 222504 (2020).

[83] C. G. Payne, S. Bacca, G. Hagen, W. G. Jiang, and T. Papenbrock, Coherent elastic neutrino-nucleus scattering on ^{40}Ar from first principles, Phys. Rev. C **100**, 061304 (2019).

[84] S. J. Novario, G. Hagen, G. R. Jansen, and T. Papenbrock, Charge radii of exotic neon and magnesium isotopes, arXiv:2007.06684 [nucl-th].